Optics Communications 468 (2020) 125791

Contents lists available at ScienceDirect

Optics Communications

journal homepage: www.elsevier.com/locate/optcom

Modelling and simulation of electromagnetically induced transparency in hollow-core microstructured optical fibres

Sílvia M.G. Rodrigues [a,*], Margarida Facão [a], M. Inês Carvalho [b], Mário F.S. Ferreira [a]

[a] Departamento de Física, Universidade de Aveiro and I3N, Campus Universitário de Santiago, 3810-193 Aveiro, Portugal
[b] DEEC/FEUP and INESC TEC, Universidade do Porto, Rua Dr. Roberto Frias, 4200-465 Porto, Portugal

ARTICLE INFO

Keywords:
Electromagnetically induced transparency
Microstructured optical fibres
Light induced phenomena
Nonlinear fibre optics
Doppler effect

ABSTRACT

We study the electromagnetically induced transparency (EIT) phenomenon in a hollow-core fibre filled with rubidium gas. We analyse the impact of the guiding effect and of the temperature on the properties of the EIT phenomenon. The refractive index felt by the probe laser is found to vary due to the radial dependence of the fibre mode field at the pump frequency. Several results are presented for the transmission, dispersion, and group velocity of the probe field, considering both the free propagation regime and the guided propagation along the hollow-core fibre. We note that the EIT occurring in a waveguide has a great potential for practical applications since it can be controlled by adjusting the gas and the fibre properties.

1. Introduction

The electromagnetically induced transparency (EIT) is a phenomena at which the presence of a control field converts an initially opaque medium into a transparent one, at certain frequencies. Theoretically, a 100% transmission can be achieved. This effect was theoretically predicted [1], and experimentally observed in the 1990's [2]. The EIT effect may be observed in a 3-level atomic system coupled to two resonant laser signals. In practice, some of the gases in which the EIT effect was observed are strontium [2,3], rubidium [4], acetylene [5], and caesium [6].

This phenomenon has several potential applications such as in the generation of ultraslow light [7], stored light [8], enhancement of nonlinear optical effects [9], lossless propagation of laser beams through optically thick media [9], and quantum information processing [10]. The materials under EIT have been considered the most nonlinear materials found up to date [11].

Actually, most of the work concerning the EIT phenomenon has been realized assuming the free propagation regime of light in some of the above mentioned gases. However, it is clear that the realization of this phenomenon in a confined medium will present some important advantages. In particular, a hollow-core microstructured optical fibre (HC-MOF) will provide a more controlled environment, including diffraction-free conditions and the possibility of beam guiding. Some possible applications of EIT in HC-MOFs include achievement of slow-light, or nonlinear optics with low-light levels.

The references [4,12,13] report experimental studies of EIT in HC-MOFs; however, in the corresponding simulations the authors did not take into account the guiding effect. In reference [14], the authors have studied the propagation of solitons in a lambda-type three-level atomic system, confined in the slot of the waveguide. In reference [15], the authors have considered soliton pulses propagation in a kagomé-structured HC-MOF, with the aim of applying it to the storage and retrieval of optical pulses.

In this work, we will numerically study the linear propagation of a probe beam interacting with a gas of rubidium enclosed in a HC-MOF in the presence of a control beam that enables the EIT. We have obtained the fundamental modes of the probe field (in a wavelength range around the resonance) considering a refractive index in the core varying accordingly to the radial dependence of the fibre mode field at the pump wavelength. Using those modes data, we were able to determine the transmission, dispersion and group velocity. We consider two cases: (i) a case that only considers relaxation processes associated with the characteristic spontaneous emission of the involved levels; (ii) another case that also considers extrinsic relaxation processes, like collisions between the atoms or between the atoms and the core fibre walls. In the latter case, we have also added the Doppler broadening effect.

Our paper is organized as follows. In Section 2, we present the theory based on the density matrix formalism. In Section 3, we present firstly some results that do not take into account the guiding effect, for comparison purposes, and then the results of transmission, dispersion and group velocity for the probe beam including the guiding effects of a HC-MOF filled with rubidium. In Section 4, we summarize the main results.

* Corresponding author.
E-mail address: silviamgr@ua.pt (S.M.G. Rodrigues).

https://doi.org/10.1016/j.optcom.2020.125791
Received 27 November 2019; Received in revised form 17 March 2020; Accepted 18 March 2020
Available online 21 March 2020

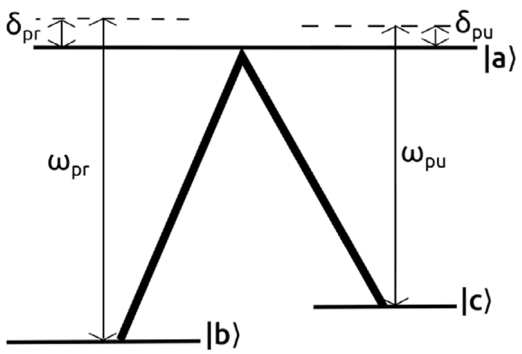

Fig. 1. The energy levels of an atom with Λ-type configuration and the probe and pump laser frequencies.

2. Theory

We will consider a three-level atomic system on a Λ-configuration as indicated in Fig. 1 associated with three atomic frequencies ω_a, ω_b and ω_c. The probe and pump lasers have frequencies $\omega_{\rm pr}$ and $\omega_{\rm pu}$, respectively, and $\delta_{\rm pr} = \omega_{\rm pr} - \omega_a + \omega_b$ and $\delta_{\rm pu} = \omega_{\rm pu} - \omega_a + \omega_c$ are the detuning of the lasers with the corresponding transitions. We assume that the light of these lasers is monochromatic.

We have followed the references [16,17]. The full Hamiltonian of the system is the sum of the Hamiltonian of the free atom with the interaction potentials of the atomic system with the two lasers:

$$H = H_0 + V_{\rm pr} + V_{\rm pu}. \tag{1}$$

where $V_{\rm pu}$ is the interaction potential with the pump field, and $V_{\rm pr}$ is the interaction potential with the probe field. The matrix form of the above Hamiltonian in the basis of the three level states is given by [17]:

$$H = \begin{bmatrix} \hbar\omega_a & \frac{\hbar\Omega_{\rm pr}}{2} e^{-i\omega_{\rm pr}t} & \frac{\hbar\Omega_{\rm pu}}{2} e^{-i\omega_{\rm pu}t} \\ \frac{\hbar\Omega_{\rm pr}}{2} e^{i\omega_{\rm pr}t} & \hbar\omega_b & 0 \\ \frac{\hbar\Omega_{\rm pu}}{2} e^{i\omega_{\rm pu}t} & 0 & \hbar\omega_c \end{bmatrix} \tag{2}$$

where $\hbar$ is the reduced Plank's constant, t is time, $\Omega_{\rm pu}$ is the Rabi frequency of the interaction of levels $|a\rangle$ and $|c\rangle$ with the pump laser, and $\Omega_{\rm pr}$ is the Rabi frequency of the interaction of levels $|a\rangle$ and $|b\rangle$ with the probe laser:

$$\Omega_{\rm pu} = -\vec{d}_{ca}.\vec{E}_{\rm pu0}/\hbar \tag{3a}$$

$$\Omega_{\rm pr} = -\vec{d}_{ba}.\vec{E}_{\rm pr0}/\hbar \tag{3b}$$

where, $\vec{d}_{ca}$ and $\vec{d}_{ba}$ are the electric dipolar moments, $\vec{E}_{\rm pu0}$ and $\vec{E}_{\rm pr0}$ are the vector amplitudes of the optical fields.

In the density matrix formalism, the dynamics of the density matrix elements can be calculated using the Liouville equation [16]:

$$\frac{d\rho}{dt} = \frac{i}{\hbar}[\rho, H] - \frac{d(\rho_{\rm relax})}{dt} \tag{4}$$

where ρ is the density matrix, and $d(\rho_{\rm relax})/dt$ is a term that describes the relaxation of ρ including effects such as population decay by spontaneous emission or energy-conserving dephasing, modelled by the decay rates γ_{ab}, γ_{cb} and γ_{ac} [16].

Assuming a steady-state regime, i.e., the state at which all the derivatives of the density matrix elements vanishes, that $\Omega_{\rm pu} \gg \Omega_{\rm pr}$, and that the population of the ground level barely decreases ($\rho_{bb} \approx 1$ and $\rho_{aa} = \rho_{cc} \approx 0$), an analytic solution can be found for each matrix element ρ_{ij}, $i \neq j$. In particular, we have:

$$\tilde{\rho}_{ab} = -i\frac{\Omega_{\rm pr}}{2}\left[\gamma_{ab} - i\delta_{pr} + \frac{(\Omega_{\rm pu}/2)^2}{\gamma_{cb} - i(\delta_{\rm pr} - \delta_{\rm pu})}\right]^{-1}. \tag{5}$$

where $\tilde{\rho}_{ab}$ is the slow variable defined as $\tilde{\rho}_{ab} = \rho_{ab}e^{i\omega_{pr}t}$. The average dipole moment of each atom due to the interaction with the probe laser is $p = d_{ab}(\rho_{ab} + \rho_{ba})$.

Considering N atoms (or molecules) per unit volume, the amplitude of the polarization vector is $P = Np$, which when compared with the linear approximation $P = \epsilon_0\chi E_{\rm pr}$ gives the following result for the susceptibility:

$$\chi = -\frac{2Nd_{ab}^2\tilde{\rho}_{ab}}{\epsilon_0\hbar\Omega_{\rm pr}}, \tag{6}$$

where ϵ_0 is the permittivity of free space. Then, using the relation $n = \sqrt{1+\chi}$ we obtain the following result for the complex refractive index, n:

$$n = \sqrt{1 + i\frac{Nd_{ba}^2}{\epsilon_0\hbar}\left[\gamma_{ab} - i\delta_{\rm pr} + \frac{(\Omega_{\rm pu}/2)^2}{\gamma_{cb} - i(\delta_{\rm pr} - \delta_{\rm pu})}\right]^{-1}}. \tag{7}$$

In this work, we have used the full expression for n above instead of an approximation that assumes that χ is small, as is usual in other references.

The real and imaginary parts of the refractive index can be obtained from Eq. (7). The imaginary part is used to compute the power transmission, with the relation:

$$T = \exp(-\alpha l) \tag{8}$$

where $\alpha = 2k_{\rm pr}\,{\rm Im}(n)$, with $k_{\rm pr} = \omega_{\rm pr}/c$, and l is the propagation length.

In this paper, we will also consider the broadening produced by the Doppler effect, due to the movements of the atoms with velocity, v_{at}.

As a result of this effect there is a change in both the probe and pump frequencies, which for $v_{\rm at} \ll c$, become:

$$\omega_{\rm pr} = \left(1 + \frac{v_{\rm at}}{c}\right)\omega_{\rm pr}^0 \tag{9}$$

$$\omega_{\rm pu} = \left(1 + \frac{v_{\rm at}}{c}\right)\omega_{\rm pu}^0 \tag{10}$$

where c is the speed of light, and $\omega_{\rm pr}^0$ and $\omega_{\rm pu}^0$ are the frequencies in the absence of the Doppler effect.

The atomic velocities have a Maxwellian distribution, which after the integration over the transverse dimensions results in the Gaussian:

$$f_\Theta(v) = \frac{1}{v_\Theta\sqrt{\pi}}e^{-(v/v_\Theta)^2}, \tag{11}$$

where $v_\Theta = \sqrt{2k_B\Theta/m}$ is the mean velocity of the atoms when the system is at temperature Θ, v is the component of the atoms velocity in the direction of the emission, k_B is the Boltzmann constant, and m is the mass of each emitting atom.

As a consequence of having multiple velocities in the system, the resultant macroscopic susceptibility χ, as well as $\tilde{\rho}_{ab}$, is given by an integral representing an average through all the velocities each with a weight, $f_\Theta(v)$, such that:

$$\tilde{\rho}'_{ab} = \int_{-\infty}^{+\infty}\tilde{\rho}_{ab}(v)f_\Theta(v)dv. \tag{12}$$

As a result, we obtain:

$$\tilde{\rho}'_{ab} = \Omega_{\rm pr}\frac{\sqrt{\pi}}{2k_{\rm pr}v_\Theta}e^{-z^2}[{\rm Erfi}(z) - i], \tag{13}$$

with $z = \left[\delta_{\rm pr}^0 + i\gamma_{ab} + \frac{\Omega_{\rm pu}^2}{4(\Delta_0 - i\gamma_{bc})}\right]/(k_{\rm pr}v_\Theta)$, where $\Delta_0 = \delta_{\rm pu}^0 - \delta_{\rm pr}^0$, $\delta_{\rm pr}^0$, and $\delta_{\rm pu}^0$ are the values in the absence of the Doppler effect. Erfi is the imaginary error function defined mathematically as ${\rm Erfi}(z) = -i{\rm Erf}(iz)$, and Erf is the real error function defined as ${\rm Erf}(z) = \frac{2}{\sqrt{\pi}}\int_0^z e^{-t^2}dt$.

Then, in order to study EIT in MOFs we have to use numerical methods. When we want to find the properties of the light propagating in a MOF we need to describe how the refractive index varies along the cross section of the fibre. For a bulk material the refractive index

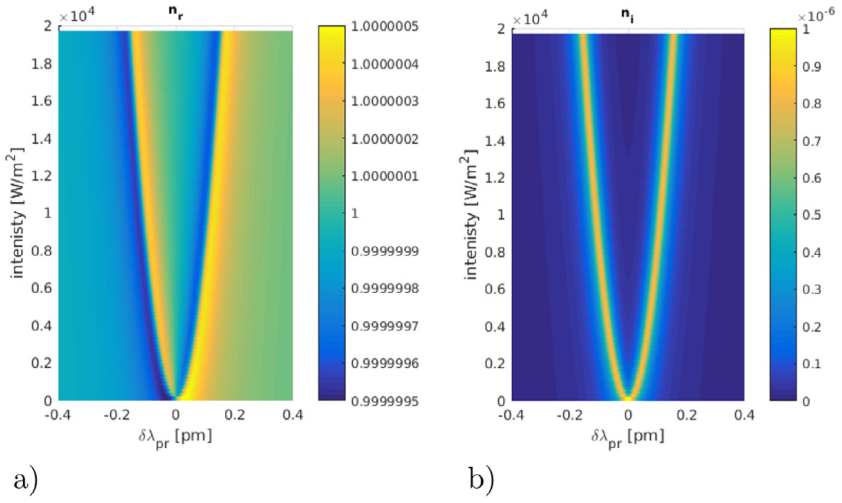

Fig. 2. Real (a) and imaginary (b) parts of the refractive index for different probe wavelengths, λ, and different intensities of the pump laser, for case 1.

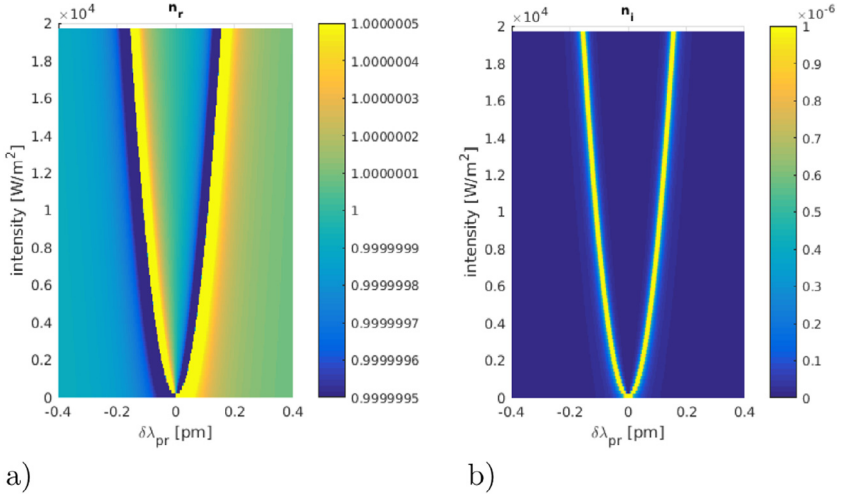

Fig. 3. Real (a) and imaginary (b) parts of the refractive index for different probe wavelengths, λ, and different intensities of the pump laser, for case 2.

is assumed to be constant on the space region; in a HC-MOF filled with rubidium and with a pump signal, the probe signal fells a refractive index that varies accordingly to Eq. (7) and Eq. (3a). Since the intensity of the fibre mode at the pump frequency varies along the radial coordinate of the fibre's core, the refractive index felt by the probe signal also depends on the radial coordinate.

For studying the guiding effects on the EIT characteristics, we have considered a photonic bandgap fibre with a hexagonal micro-structured cladding made of silica. The pitch and hole diameters are 4.0 μm and 3.9 μm, respectively.

The properties of the light propagation in a MOF are described by the Helmholtz equation:

$$\nabla \times \left[\frac{1}{\epsilon_r(\mathbf{r},\lambda)}\nabla \times \mathbf{H}(\mathbf{r},\lambda)\right] = \left(\frac{\omega}{c}\right)^2 \mathbf{H}(\mathbf{r},\lambda); \tag{14}$$

$$\mathbf{E}(\mathbf{r},\lambda) = \frac{i}{\omega\epsilon_0\epsilon_r(\mathbf{r},\lambda)}\nabla \times \mathbf{H}(\mathbf{r},\lambda); \tag{15}$$

where the relative magnetic permeability was assumed equal to one and ϵ_r is the electric permittivity such that $n^2 = \epsilon_r$. Eq. (14) is also known as the master equation [18] with which we can find the fibre modes, assuming a relative electric permittivity ϵ_r in each point of the fibre cross-section. After solving Eq. (14), we obtain the optical field distribution with the Eq. (15). With these two equations we can obtain the optical guided modes and the corresponding propagation constant of a mode on an optical fibre.

For the purpose of solving Eq. (14), we need to describe the distribution of the refractive index, n, in the transverse section of the fibre to obtain the fibre's properties. We have considered that distinct materials were present in the fibre's cross section: The expression in Eq. (7) for a Λ-system, such as the rubidium gas, was considered in the fibre's core material. Moreover, we have taken into account the radial dependence of the fibre mode at the pump wavelength through the expression for the pump profile with $\Omega_{\text{pu}} \equiv \Omega_{\text{pu}}(r)$ [see Eq. (17)]; We have considered the refractive index of silica, n_{silica}, for the strands of the fibre's cladding; The holes of the cladding were assumed to be filled by air, with a refractive index $n_{\text{air}} \approx 1.00029$.

The refractive index of silica was calculated with a Sellmeier equation [19, chapt. 2]:

$$n = \sqrt{1 + \sum_j \frac{a_j \lambda^2}{\lambda^2 - b_j}}, \tag{16}$$

whose assumed coefficients correspond to 3 terms: $a_1 = 0.6965325$, $a_2 = 0.4083099$, $a_3 = 0.8968766$, $b_1 = 0.004368309$, $b_2 = 0.01394999$, and $b_3 = 97.93399$, as in Ref. [20, chapt. 3].

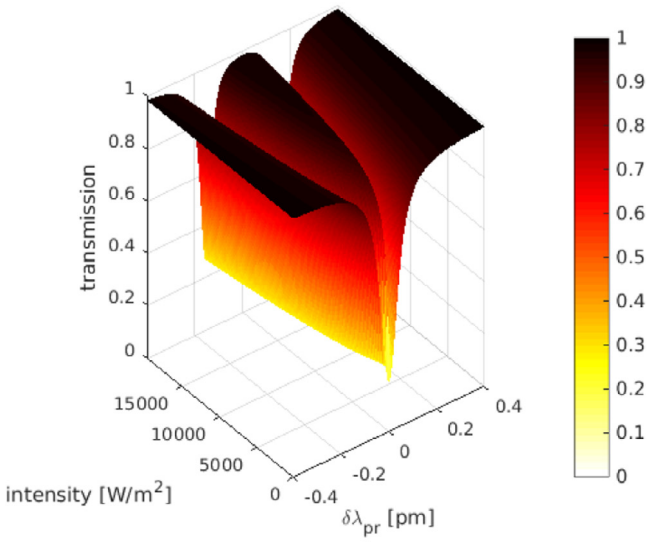

(a)

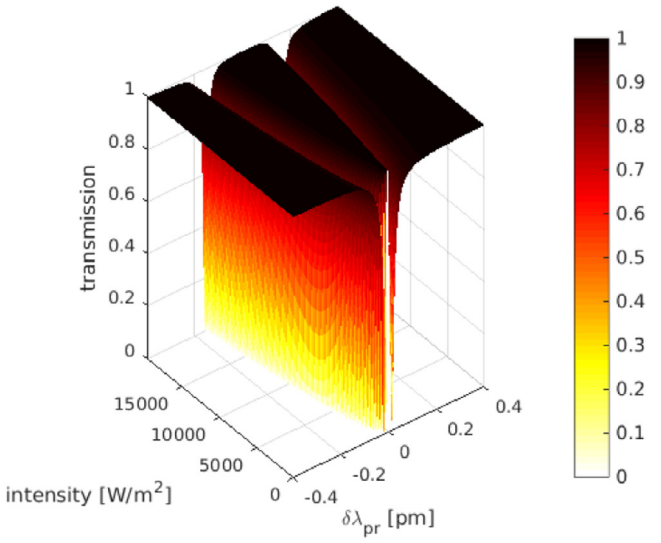

(b)

Fig. 4. Transmission for free propagation along a distance of 10 cm, considering different intensities of the pump field for: (a) case 1, and (b) case 2.

3. Results

We have considered a gas of rubidium and its energy levels $^5S_{1/2}$ $F = 1$, $^5S_{1/2}$ $F = 2$ and $^5P_{1/2}$ as $|b\rangle$, $|c\rangle$ and $|a\rangle$, respectively [21]. These transitions correspond to: λ_{ba}=0.794969846 μm for the probe transition, and λ_{ca}=0.794984254 μm for the pump transition. The electric dipolar moments of those transitions are $d_{ba} = d_{ca} = 2.54 \times 10^{-29}$ Cm. In all the simulations, we considered the density of atoms equal to $N = 2.73 \times 10^{14}$ m^{-3} (with values close to Ref. [22]), and that the pump field was perfectly resonant with the transition $|a\rangle|c\rangle$, i.e, $\delta_{pu} = 0$. The detuning of the probe was studied in several sections of our paper.

At a realist setup the collisions between atoms and of the atoms with the fibre-core walls will increase the decoherence rates in a way that will depend on the experimental conditions. In our study, we intended to use typical values for these rates, so we have considered the following for the case 1: $\gamma_{ij} = 90$ MHz for the decoherence rates between levels for which the transitions are dipole allowed ($|a\rangle$ and $|b\rangle$, and $|a\rangle$ and $|c\rangle$); and $\gamma_{ij} = 24$ MHz for the decoherence rates between levels for which the transitions are dipole prohibited ($|b\rangle$ and $|c\rangle$). These are typical values for room temperature EIT experiments, following those reported with the experimental setup of Ref. [4].

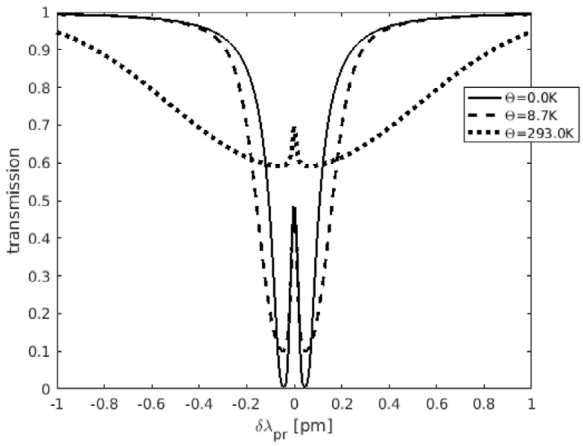

Fig. 5. Transmission on 40 cm long path (for case 1), and Doppler effect for different temperatures (note we have checked that the results for $\Theta = 0.0$ K with or without Doppler coincide, as expected).

In addition, we have also considered a case 2 (without collisions) for which the decay and decoherence rates where taken from Ref. [21], that are the intrinsic parameters of rubidium levels. Thus, in the case 2 we have considered $\gamma_{ab} = 18.065 \times 10^6 \text{s}^{-1}$, and $\gamma_{bc} = 0$, which are the theoretical limits with minimum collisions [21]. We have considered $\gamma_{ac} \approx \gamma_{ab}$ in both cases, however γ_{ac} does not affect the results.

We will study, at first, situations without guidance, and after that we will compare both situations with and without guidance. Fig. 2(a)–(b) shows the real and imaginary parts of the refractive index, n, for different probe wavelengths and different intensities of the pump laser, for a system with collisions. We observe that the imaginary component is symmetrical relatively to the centre wavelength, which is not the case for the real component. For each specific pump intensity, we observe in Fig. 2(a) the existence of a minimum and a maximum both at the left- and at the right-hand sides. In Fig. 2(b) we observe a maximum of the imaginary component at each side of the graph, which corresponds to high losses. In the centre of this graph, assuming a pump intensity different from zero, there is a minimum of the imaginary part of n, which corresponds to a minimum of loss. Fig. 3(a)–(b) show that the case with minimum collisions has the overall shape with more pronounced minimums and maximums.

Fig. 4 shows the dependence of the probe transmission on the pump intensity and on the probe wavelength for the case 1 and the case 2, considering the free propagation along a distance of 10 cm. These graphs are computed from data such as in Fig. 2(b) and in Fig. 3(b), considering the selected distance. The minimum of the imaginary component of n at the centre probe wavelength leads to the high transmission characteristic of the EIT phenomena. We observe that the width of the EIT transmission window created around the resonance wavelength increases while increasing the pump intensity. Moreover, in the case 2, a flat profile with 100.0% transmission is achieved.

In the following we consider that the pump has an intensity $I_{\text{pu}} = 1536.4$ Wm^{-2}, which corresponds to a total power in the fibre's cross section of 78 nW. In Fig. 5, we show how the Doppler effect changes the transmission curve. The absorption curve widens in general and the EIT transmission window is not so pronounced.

Then, we proceed by studying the impact of the guidance. In our simulations, the fibre's core was assumed to be filled with rubidium but the fibre's cladding holes were filled with air. Note that we have first computed the mode for the pump field on the same fibre but assuming a core refractive index $n = 1$ and at the resonant wavelength with

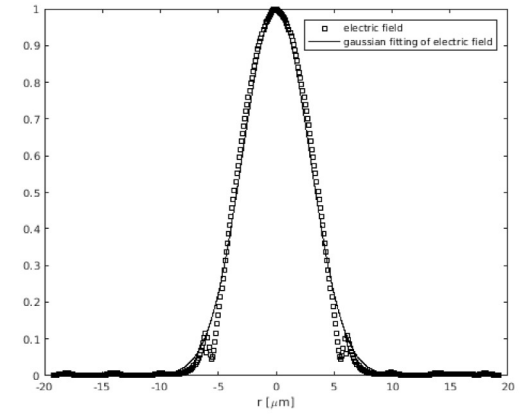

(a)

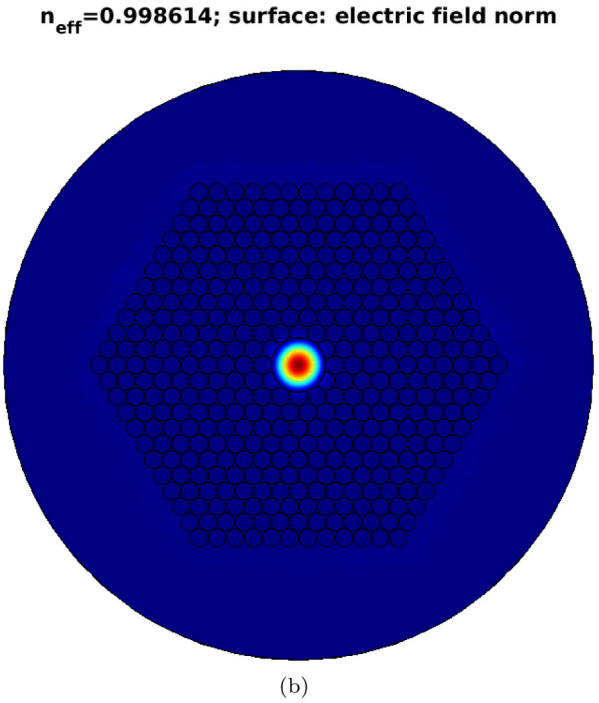

(b)

Fig. 6. (a) Amplitude of the normalized electric field as a function of the radial coordinate, r, of the fibre's fundamental mode at the pump wavelength, and its approximation by a Gaussian function; (b) Fundamental mode of the fibre due to the probe field for $\lambda_{\mathrm{pu}} = \lambda_{\mathrm{pu0}} \approx \lambda_{\mathrm{pr}} = \lambda_{\mathrm{pr0}}$, i.e. with the pump and the probe lasers at perfect resonance conditions.

levels $|a\rangle$ and $|c\rangle$. This is justified by the fact that since level $|c\rangle$ is not initially populated, the pump signal propagates as if it is in the vacuum. Then we computed the modes for the probe signal assuming a complex refractive index as in Eq. (7) with $\Omega_{\mathrm{pu}} \equiv \Omega_{\mathrm{pu}}(r)$.

Fig. 6(a) shows that the optical field of the fundamental mode has approximately a Gaussian distribution. Since the Rabi frequency is proportional to the optical pump field, as indicated by Eq. (3a), it can be described in the form:

$$\Omega_{pu} = \Omega_{pu}^{0} \exp\left\{-\left(\frac{r}{c_0}\right)^2\right\}. \tag{17}$$

In this function c_0 is a parameter which is related to the width of the Gaussian function. A value $c_0 = 4.083$ was obtained by an adjustment to the fibre mode at the pump wavelength profile, as in Fig. 6(a). As a consequence of the radial dependence of Ω_{pu}, the refractive index felt by the probe signal, given by Eq. (7), also presents a radial dependence.

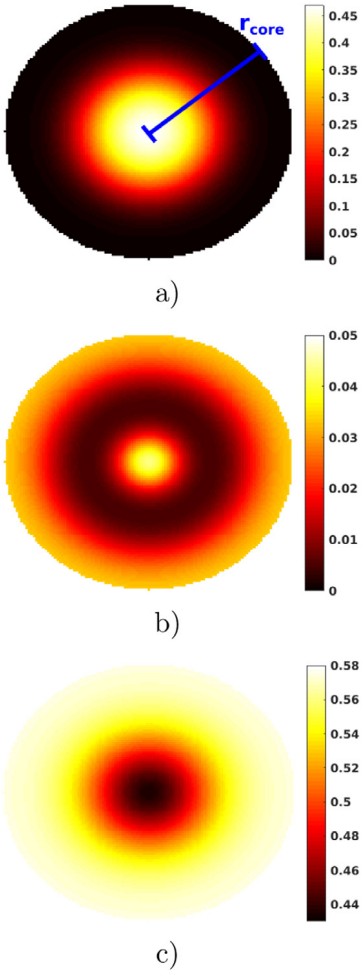

Fig. 7. Transverse distribution of the local transmission in the core of the HC-MOF, for probe wavelengths such that: (a) $\delta\lambda = 0.00$ pm; (b) $\delta\lambda = 0.03$ pm; and (c) $\delta\lambda = 0.10$ pm.

The radial variation of the mode intensity from $r = 0$ to $r = r_{core}$ for a fibre core filled by a rubidium gas has several consequences. In Fig. 6(b) we show the fundamental propagation mode for the probe field, when the pump mode is as in Fig. 6(a), and the probe laser is at perfect resonance. We observe that the light is well confined in the fibre's core.

In particular, we have a "local transmission" distinct for different values of r, as seen in Fig. 7: (a) with the probe laser at perfect resonance; (b) with the probe laser close to the resonance, with detuning of $\delta\lambda = \pm 0.03$ pm (note the transmission has a symmetrical behaviour relatively to the centre wavelength in EIT); and (c) with the probe laser far from resonance, with detuning of $\delta\lambda = \pm 0.10$ pm, whose transmission is identical for both plus ans less signal's cases, because the same symmetry discussed above.

These novel results shown here in Fig. 7 can be understood based on Fig. 2(b), and on Fig. 3(b), by considering the impact of the pump intensity variation with the radial coordinate of the fibre's core, r. For a fixed wavelength, increasing r from $r = 0$ to r_{core} means reducing the pump intensity from $\max(I_{pu})$ to ≈ 0, which corresponds to moving down along a vertical line in Fig. 2(b). In particular, in the case (a), for $\lambda_{pr} = \lambda_{pr0}$, we see that the local transmission decreases with r, which is due to the monotonous increase of the imaginary part of n; in the case (b), for $\lambda_{pr} \approx \lambda_{pr0}$, by increasing r, the imaginary part of the refractive index begins increasing until reaching a maximum value, after which it decreases again; in the case (c), for $|\lambda_{pr} - \lambda_{pr0}| \gg 0$, the variation of the

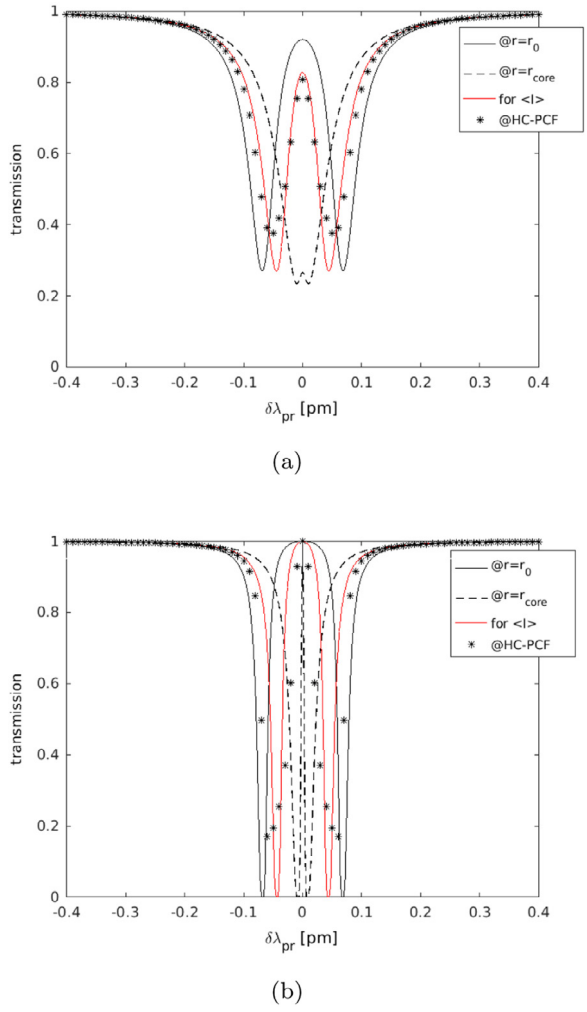

Fig. 8. Transmission for (a) case 1, and (b) case 2 after 10 cm of fibre and over a 10 cm path without guiding but different Ω_{pu} as indicated in the legend.

transmission is opposite to that observed in the case (a), which is due to the impact of the variation of pump intensity far from resonance.

In Fig. 8(a)–(b), we show the transmission along 10 cm of fibre for cases 1 and 2, respectively. For comparison purposes, we have added the curves without guiding assuming three different constant values for Ω_{pu}: the peak value of $\Omega_{pu}(r)$ that occurs at $r = 0$, the value of $\Omega_{pu}(r)$ at $r = r_{core}$, and $\bar{\Omega}_{pu}$ that is its average over the core. With these figures, we may see that the guiding lead to a transmission curve close to the curve for $\bar{\Omega}_{pu}$. In both cases, we still observe the transmission window.

The continuous black curve of Fig. 8(a) [i.e. for $r = 0$], and the continuous black curve of Fig. 8(b) are included in Fig. 4 for a fixed $I_{pu} = 1536.4\ \mathrm{Wm}^{-2}$.

Then, we added the Doppler effect such that Figs. 9(a), 9(b) and 9(c) show the transmission, dispersion and group velocity for case 1, at $\Theta = 0$ K and $\Theta = 293$ K. We note differences between the free propagation and the guided propagation [Fig. 9(a)–(c)]. In particular, the differences are more pronounced when $\Theta = 0$ K.

In Fig. 9(a), we have included a zoom-in of the curves of Fig. 4 for the free propagation at the two selected temperatures of 0 K and 293 K, as well as two curves with the guidance effect. In the middle of the EIT window, for the temperature of 0 K, we obtain a transmission of 47.0% in the case of free propagation, and a transmission of 42.4% in the case of guided light. Thus, we observe that in the case of $\Theta = 0$ K the transmission is slightly lower with guidance. However, in the case of $\Theta = 293$ K the transmission is slightly higher with guidance (70.5%) compared with the free propagation (69.1%).

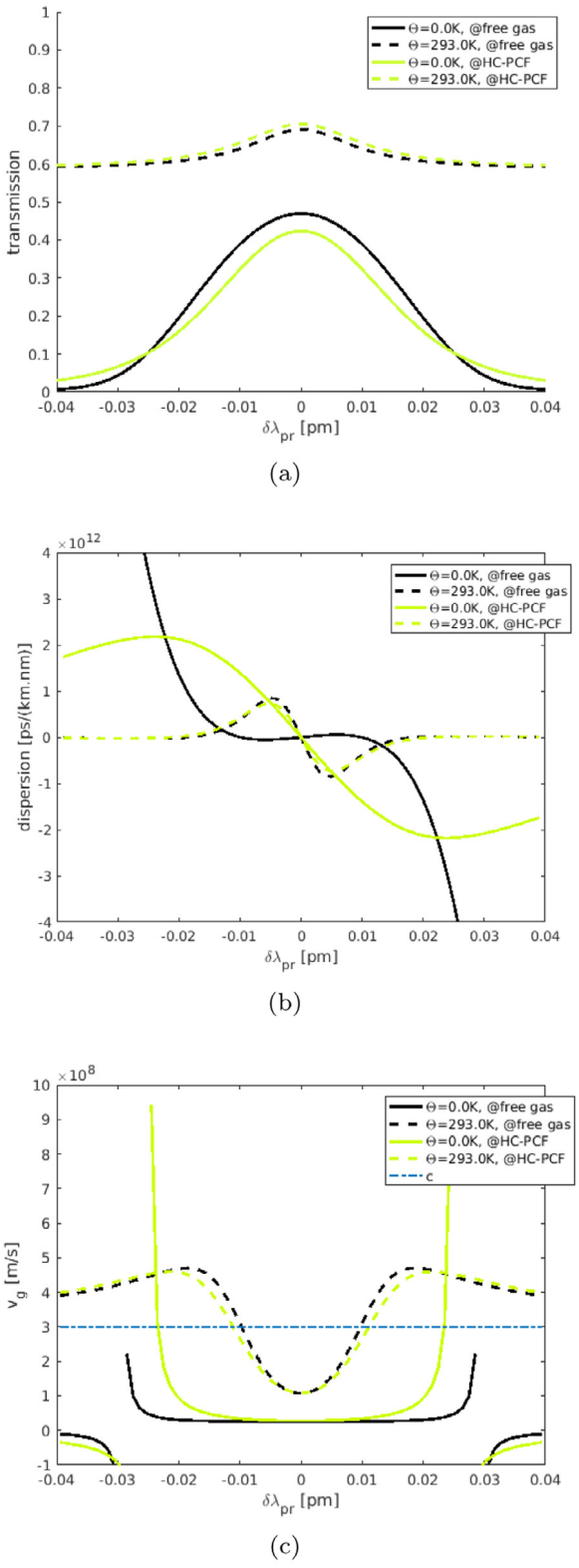

Fig. 9. (a) Transmission after 40 cm, (b) dispersion, and (c) group velocity for case 1, without Doppler ($\Theta = 0$ K) and considering Doppler ($\Theta = 293.0$ K), for both in guided and in free rubidium.

In the case of the free propagation we have a flat dispersion at the middle point for $\Theta = 0$ K, whereas in the case of guidance we have a dispersion curve with a negative slope [Fig. 9(b)]. Moreover, the amplitude of the dispersion variation is smaller in the case of guidance,

which can be an advantage for the light propagation within a large range of wavelengths. For the room temperature, the dispersion is less affected by the guidance.

Fig. 9(c) shows that, in all cases, the centre of the EIT window permits slow light, while in the side-bands of the EIT window, the conditions are favourable for fast light. In particular, we note that for $\Theta = 0$ K there are discontinuities at the side-bands, whereas the two curves for $\Theta = 293$ K are continuous and similar.

4. Conclusions

Using a semi-classical approach for EIT, we have considered the resulting complex refractive index for two relaxation regimes, with collisions and without collisions. Moreover, we have also studied the impact of the Doppler broadening. We obtained general results for a probe beam propagating through the gas without any confinement and then we compared these results with ones obtained considering the propagation in a HC-MOF. For that purpose, we use the complex refractive index but admitting a Gaussian radial dependence of the pump Rabi frequency. Our results show that for very low temperatures the transmission, dispersion and group velocity are different for the free propagation and the propagation inside the fibre. However, at room temperatures the results do not differ significantly in the two cases. This new simulation approach may be useful to search for engineered conditions of EIT.

Funding information

This work was financed by National Funds through the Portuguese funding agency, FCT — Fundação para a Ciência e a Tecnologia, Portugal, within the projects: UID/EEA/50014/2019 and UID/CTM/50025/2019, and the research grants: PD/BI/52527/2014, PD/BD/108650/2015, and "BI-14 (7409/2018)".

Declaration of competing interest

The authors declare that they have no known competing financial interests or personal relationships that could have appeared to influence the work reported in this paper.

CRediT authorship contribution statement

Sílvia M.G. Rodrigues: Methodology, Software, Formal analysis, Investigation, Writing - original draft. **Margarida Facão:** Methodology, Validation, Writing - review & editing. **M. Inês Carvalho:** Methodology, Validation, Writing - review & editing. **Mário F.S. Ferreira:** Conceptualization, Writing - review & editing, Supervision.

References

[1] S.E. Harris, J.E. Field, A. Imamoglu, Nonlinear optical processes using electromagnetically induced transparency, Phys. Rev. Lett. 64 (1990) 1107.
[2] K.J. Boller, A. Imamoglu, S.E. Harris, Observation of electromagnetically induced transparency, Phys. Rev. Lett. 66 (20) (1991) 2593–2596.
[3] S.E. Harris, Electromagnetically induced transparency, Phys. Today 50 (7) (1997) 36.
[4] S. Ghosh, A.R. Bhagwat, C.K. Renshaw, S. Goh, A.L. Gaeta, B.J. Kirby, Low-light-level optical interactions with rubidium vapor in a photonic band-gap fiber, Phys. Rev. Lett. 97 (2) (2006) 023603.
[5] N.V. Wheeler, P.S. Light, F. Couny, F. Benabid, EIT-based slow and fast light in an all-fiber system, in: Proc. SPIE 7612, Advances in Slow and Fast Light III (0), 2010.
[6] D. Wang, J.Z. Wu, J.X. Zhang, Optical control of light propagation in photonic crystal based on electromagnetically induced transparency, Chinese Phys. B 25 (6) (2016) 064202.
[7] S.E. Harris, L.V. Hau, Nonlinear optics at low light levels, Phys. Rev. Lett. 82 (1999) 4611–4614.
[8] D.F. Phillips, A. Fleischhauer, A. Mair, R.L. Walsworth, M.D. Lukin, Storage of light in atomic vapor, Phys. Rev. Lett. 86 (2001) 783–786.
[9] J.P. Marangos, Topical review: electromagnetic induced transparency, J. Modern Opt. 45 (3) (1998) 471–503.
[10] M.D. Lukin, A. Imamoğlu, Controlling photons using electromagnetically induced transparency, Nature 413 (2001) 273.
[11] M. Soljacić, J.D. Joannopoulos, Enhancement of nonlinear effects using photonic crystals, Nature Mater. 3 (2004) 211–219.
[12] F. Benabid, P. Light, F. Couny, P. Russell, Electromagnetically-induced transparency grid in acetylene-filled hollow-core PCF, Opt. Express 13 (2005) 5694–5703.
[13] S. Ghosh, J.E. Sharping, D.G. Ouzounov, A.L. Gaeta, Resonant optical interactions with molecules confined in photonic band-gap fibers, Phys. Rev. Lett. 94 (2005) 093902.
[14] J. Xu, G. Huang, Electromagnetically induced transparency and ultraslow optical solitons in a coherent atomic gas filled in a slot waveguide, Opt. Express 21 (2013) 5149–5163.
[15] D. Xu, Z. Chen, G. Huang, Ultraslow weak-light solitons and their storage and retrieval in a kagome-structured hollow-core photonic crystal fiber, Opt. Express 25 (16) (2017) 19094–19111.
[16] Y.R. Shen, The Principles of Nonlinear Optics, first ed., Wiley-Interscience, 2002.
[17] G.T. Purves, Absorption and dispersion in atomic vapours: applications to interferometery (Ph.D. thesis), Dep. of Physics, University of Durham, 2006.
[18] J.D. Joannopoulos, S.G. Johnson, J.N. Winn, R.D. Meade, Photonic Crystals: Molding the Flow of Light, second ed., Princeton University Press, 2008.
[19] M.F.S. Ferreira, Nonlinear Effects in Optical Fibers, first ed., John Wiley & Sons - OSA, 2011.
[20] K. Okamoto, Fundamentals of Optical Waveguides, second ed., Academic Press, 2005.
[21] D.A. Steck, Rubidium 87 d line data, Technical report, 2010, Online at http://steck.us/alkalidata (revision 2.1.4, 23 December 2010).
[22] S.A. Hopkins, E. Usadi, H.X. Chen, A.V. Durrant, Electromagnetically induced transparency of laser-cooled rubidium atoms in three-level Λ-type systems, Opt. Commun. 138 (1997) pp. 185–192.